AFRL-AFOSR-JP-TR-2017-0078

Investigation of Chirality Selection Mechanism of Single-Walled Carbon Nanotube-3

Seun Min Kim
KOREA INSTITUTE OF SCIENCE AND TECHNOLOGY (KIST)

12/14/2017
Final Report

Air Force Research Laboratory
AF Office Of Scientific Research (AFOSR)/ IOA
Arlington, Virginia 22203
Air Force Materiel Command

REPORT DOCUMENTATION PAGE

Form Approved
OMB No. 0704-0188

1. REPORT DATE *(DD-MM-YYYY)*	2. REPORT TYPE	3. DATES COVERED *(From - To)*
14-12-2017	Final	22 Sep 2016 to 21 Dec 2017

4. TITLE AND SUBTITLE
Investigation of Chirality Selection Mechanism of Single-Walled Carbon Nanotube-3

5a. CONTRACT NUMBER

5b. GRANT NUMBER
FA2386-16-1-4059

5c. PROGRAM ELEMENT NUMBER
61102F

6. AUTHOR(S)
Seun Min Kim

5d. PROJECT NUMBER

5e. TASK NUMBER

5f. WORK UNIT NUMBER

7. PERFORMING ORGANIZATION NAME(S) AND ADDRESS(ES)
KOREA INSTITUTE OF SCIENCE AND TECHNOLOGY (KIST)
39-1 HAWEOLGOK-DONG, SUNGBUK-KU
SEOUL, 136-791 KR

8. PERFORMING ORGANIZATION REPORT NUMBER

9. SPONSORING/MONITORING AGENCY NAME(S) AND ADDRESS(ES)
AOARD
UNIT 45002
APO AP 96338-5002

10. SPONSOR/MONITOR'S ACRONYM(S)
AFRL/AFOSR IOA

11. SPONSOR/MONITOR'S REPORT NUMBER(S)
AFRL-AFOSR-JP-TR-2017-0078

12. DISTRIBUTION/AVAILABILITY STATEMENT
A DISTRIBUTION UNLIMITED: PB Public Release

13. SUPPLEMENTARY NOTES

14. ABSTRACT
In this project final report, the PI described a new method to improve carbon nanotube (CNT) array growth by the rational design of the catalyst layer. The PI adapted Fe ion implantation as a new catalyst deposition method. The PI tested the performance of Fe-implanted wafer as catalyst for CNT forest growth and, unlike catalysts formed from PVD method, it was confirmed that the catalysts formed on Fe-implanted wafer maintain their size and number density even after prolonged growth duration. As a result, the Fe-implanted wafer is effective in (1) growth of CNT forests having uniform diameter distribution and (2) growth of tall CNT forests by maintaining the number density of catalysts during the growth. The PI also has 1 peer reviewed paper as a result of the grant titled: Synthesis of CNT forest with narrow diameter distribution from the Fe ion implanted wafer, Carbon, vol. 123, pp. 122-128 (2017).

15. SUBJECT TERMS
Carbon Nanotubes, Catalysis, Chirality, Processing, Mechanism, Growth Termination, Morphology

16. SECURITY CLASSIFICATION OF:			17. LIMITATION OF ABSTRACT	18. NUMBER OF PAGES	19a. NAME OF RESPONSIBLE PERSON
a. REPORT	b. ABSTRACT	c. THIS PAGE			CHEN, JERMONT
Unclassified	Unclassified	Unclassified	SAR	18	19b. TELEPHONE NUMBER *(Include area code)* 315-227-7007

Final Report for AOARD Grant FA2386-16-1-4059

"Investigation of chirality selection mechanism of single-walled carbon nanotube_3"

Date: 12/13/2017

PI and Co-PI information:

- Name of Principal Investigator: Seung Min Kim
- E-mail address: seungmin.kim@kist.re.kr
- Institution: Korea Institute of Science and Technology
- Department: Carbon Composite Materials Research Center
- Mailing Address: Chudong-ro 92, Bongdong-eup, Wanju-gun, Jeonbuk 55324, South Korea
- Phone: +82-63-219-8154
- Fax: +82-63-219-8419

Period of Performance: 09/22/2016 ~ 09/21/2017

Abstract:

In the third year of the project, we have more focused on the research for the improvement of carbon nanotube (CNT) array growth by the rational design of the catalyst layer. For this purpose, we have adapted Fe ion implantation as a new catalyst deposition method. We have investigated Fe ion implantation method in two ways. First, we directly synthesized CNT forests from the catalyst particles formed by the diffusion of Fe ions without any additional deposition of Fe catalyst layer. By annealing the Fe-implanted SiO_2/Si wafer in an Ar atmosphere at 800 °C for 15 min, the Fe particles on the surface of SiO_2 layer are successfully formed by the diffusion of Fe atoms from the SiO_2 layer. Interestingly, the size distribution of Fe catalyst particles for Fe-implanted SiO_2/Si wafers does not change with the prolonged annealing durations of up to 12 h. Using secondary ion mass spectroscopy and transmission electron microscopy (TEM), we confirmed that the implanted Fe atoms diffuse out of the SiO_2 layer and form Fe particles on both the SiO_2 surface and the interface between SiO_2 and Si. The cross-sectional TEM images indicate that the Fe catalyst particles are anchored in the SiO_2 layer, which limits the particles' mobility and results in an invariant catalyst size distribution for prolonged annealing durations.

Second, the Fe implanted wafer was used for delaying the growth termination. Fe ions were implanted into Al_2O_3 (10 nm) / SiO_2 / Si wafer and then thin Fe film (1 nm) was deposited on the substrate by e-beam evaporation. While the growth was decelerated on Fe-deposited wafer without Fe implantation after 5 h of growth, the growth rate was well maintained on Fe-implanted-and-

deposited wafer until the growth was terminated by the limited space of quartz tube reactor. The final length of CNT forest reached 21 mm with a potential to grow taller.

Thus, we conclude that the proposed catalyst design including Fe implantation is effective for maintaining the size and number density of catalyst particles, which is highly desirable for the growth of uniform and tall CNT forests.

Introduction:

The key lesson from the research of previous years' is that maintaining the catalyst number density is essential in the stable growth of CNT forests. We have demonstrated that catalyst loss by their various migrations including Ostwald ripening [1], sub-surface diffusion [2], and upward migration [3] can cause the termination of CNT forest growth.

In fact, all these problems have something to do with catalyst preparation method. So far, most works on the synthesis of CNT forests have highly relied on a single method for catalyst preparation—physical vapor deposition (PVD) of a catalyst thin film on a substrate by thermal evaporation, e-beam evaporation, or sputtering. The PVD method is very simple and produces catalyst films with uniform thickness, and big advancements in CNT forest growth have been made as a result; however, several universal and intrinsic problems remain. First, since the dewetting of a thin catalyst film into particles upon heating is a random process, catalyst particles with a wide size distribution are usually formed on the substrate [4]. Second, at high temperatures, catalyst particles agglomerate by particle collision [5, 6] and coarsen by Ostwald ripening [1, 7], which lead to even broader distribution of their size during the CVD synthesis of CNT forests. Third, morphological evolution of catalyst particles induced by Ostwald ripening [1], sub-surface diffusion [2], and upward migration [3] results in the depletion of catalyst particles, gradual density decay of CNTs, and eventually termination of the growth of CNT forests [8].

In order to overcome these problems, development of new catalyst preparation method is necessary. In the third year of the project, we have tested the performance of Fe-implanted wafer as catalyst for CNT forest growth. We found that, unlike catalysts formed from PVD method, it was confirmed that the catalysts formed on Fe-implanted wafer maintain their size and number density even after prolonged growth duration. As a result, the Fe-implanted wafer is effective in (1) growth of CNT forests having uniform diameter distribution and (2) growth of tall CNT forests by maintaining the number density of catalysts during the growth.

Experimental:

- Preparation of Fe ion implanted wafers

The Fe ion implanted substrate was prepared using silicon (100) wafer with a 300 nm-thick oxidized layer. Fe^+ ion was implanted using a lab-made ion implanter at the accelerating voltage of 60 keV at Korea Multi-Purpose Accelerator Complex. The dose of Fe^+ ion was $10^{16}/cm^2$. As a control sample, 1 nm-thin Fe film was deposited on a silicon (100) wafer with a 300 nm-thick oxidized layer by e-beam evaporation. For annealing, a quartz tube furnace (Lindberg/Blue M, HTF55322C, inner diameter 35 mm) was used. The Fe implanted and deposited samples were heated to 800 °C in 15 minutes under Ar atmosphere, maintained for various times, and cooled down to room temperature.

- Annealing of Fe-implanted substrates

For annealing, a quartz tube furnace (Lindberg/Blue M, HTF55322C, inner diameter 35 mm) was used. The temperature was ramped to the target temperature in 25 min under Ar atmosphere, and the temperature was maintained under Ar or Ar/H_2 atmosphere for 10 min. The samples were removed after cooling down the furnace below 100 °C under Ar gas flow.

- Growth of CNT forests on Fe-deposited substrates and Fe-implanted substrates

CNT forests were grown on the annealed wafers using the same furnace. The temperature was ramped up to 630 °C in 15 min under an Ar flow at 500 sccm. When the temperature reached 630 °C, a gas mixture of Ar (286 sccm) and C_2H_2 (19 sccm) was fed into the chamber for 10 s, followed by a gas mixture of Ar (286 sccm), C_2H_2 (19 sccm), and H_2 (95 sccm) for 3 min. The furnace was then switched off and the substrates were removed after the reactor was cooled to <100 °C under an Ar gas flow.

- Growth of tall CNT forests on Fe-deposited substrates and Fe-implanted-and-deposited substrates

The substrate was located 12 cm downstream from the middle of the tube reactor. Then the reactor was heated to 820 °C over 15 min with flowing Ar gas. During the ramping process, H_2 gas was supplied together with Ar when the temperature passed through 725°C. When the temperature reached 820°C, a gaseous mixture of Ar, H_2, C_2H_4, and ethanol vapor with Ar carrier gas was introduced and the synthesis was carried out. C_2H_4 was used as the carbon source and ethanol was used to enhance the growth and prolongs the catalyst lifetime since it decomposes into active carbon species and H_2O [9]. The volumetric ratio was Ar: H_2: C_2H_4 = 5: 10: 2. The heater

was turned off after the reaction and the substrate was removed after it had cooled to below 200 °C under an Ar gas flow.

Results and Discussion:

- Synthesis of CNT forests with narrow diameter distribution using Fe-implanted wafer

Fig. 1 shows schematic representations of different types of CNT forest growth behavior on an Fe-deposited SiO_2/Si wafer (hereafter referred to as DW, Fig. 1(a)) and an Fe-implanted SiO_2/Si wafer (hereafter referred to as IW, Fig. 1(b)). When a DW is heated to a sufficiently high temperature, the deposited Fe film starts to transform into individual particles, which can act as catalysts for the growth of the CNT forest. The formed Fe particles have a wide distribution of diameters [6], which represents the inherent limitation of the PVD method. The catalyst particles are formed by dewetting of a thin film, which is known to be a random process. In addition, the morphology of the formed particles continue to evolve during subsequent annealing and CNT growth due to Ostwald ripening [2, 7, 10, 11] and particle migration [12-14]. The non-uniform diameters of the Fe particles result in the growth of CNTs with a wide diameter distribution. In order to overcome this limitation of PVD, the method of Fe ion implantation can be utilized as an alternative to prepare the Fe catalyst particles for CNT forest growth. When Fe ions are implanted into the SiO_2/Si wafer, they form Fe particles inside the SiO_2 layer on Si [15, 16]. Upon annealing, the Fe particles are expected to diffuse out of interior of the SiO_2 layer to the surface [17] and be distributed like floating icebergs embedded in the SiO_2 layer. As a result, the embedded particles are expected to have a limited mobility on the surface of the SiO_2 layer, so the size distribution of the particles is likely to be maintained even after prolonged annealing. This characteristic of the ion implantation method is expected to be beneficial to growing CNTs with uniform diameters.

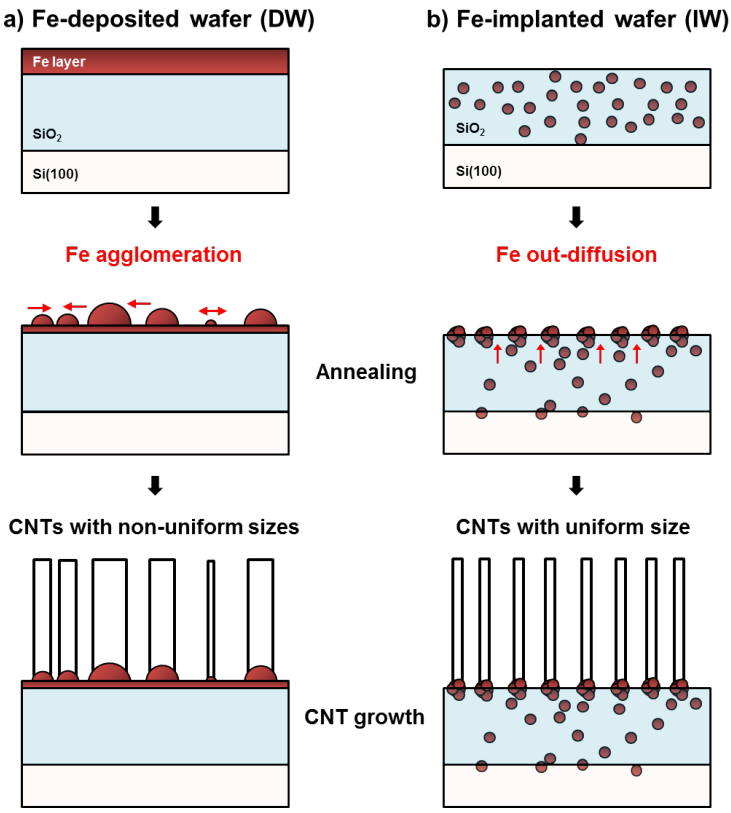

Fig. 1. Schematic diagram of the growth of CNT forests on (a) an Fe-deposited wafer (DW), and (b) an Fe-implanted wafer (IW).

In order to confirm the above hypothesis, the size distribution of Fe catalyst particles in various IWs was measured after they were subjected to thermal annealing durations of 15 min, 1 h, 4 h, and 12 h at 800 °C in Ar and H_2 atmospheres. For comparison, Fig. 2(a) shows the AFM image of the DW after it was annealed for 15 min at 800 °C in an Ar atmosphere, and Fig. 2(b) is the particle size distribution obtained from the image in Fig. 2(a). After only 15 min of annealing, the particle size distribution already becomes very broad (ranging from several namometers to 100 nm) and several peaks appear. However, for the IW annealed for 15 min in Ar, the particle size distribution is much narrower than that of the DW, as shown in Fig. 2(c) and (d). Fig. 2(c)–(j) show the evolution in the size distribution of Fe particles in IW samples that were annealed at 800 °C in Ar for 15 min to 12 h. Surprisingly, the size distribution of Fe particles in the IWs remain almost unchanged with increasing annealing durations. There are few particles that are larger than 50 nm even after 12 h of annealing. All of the particle size distributions show a single peak, and the peak positions are nearly identical.

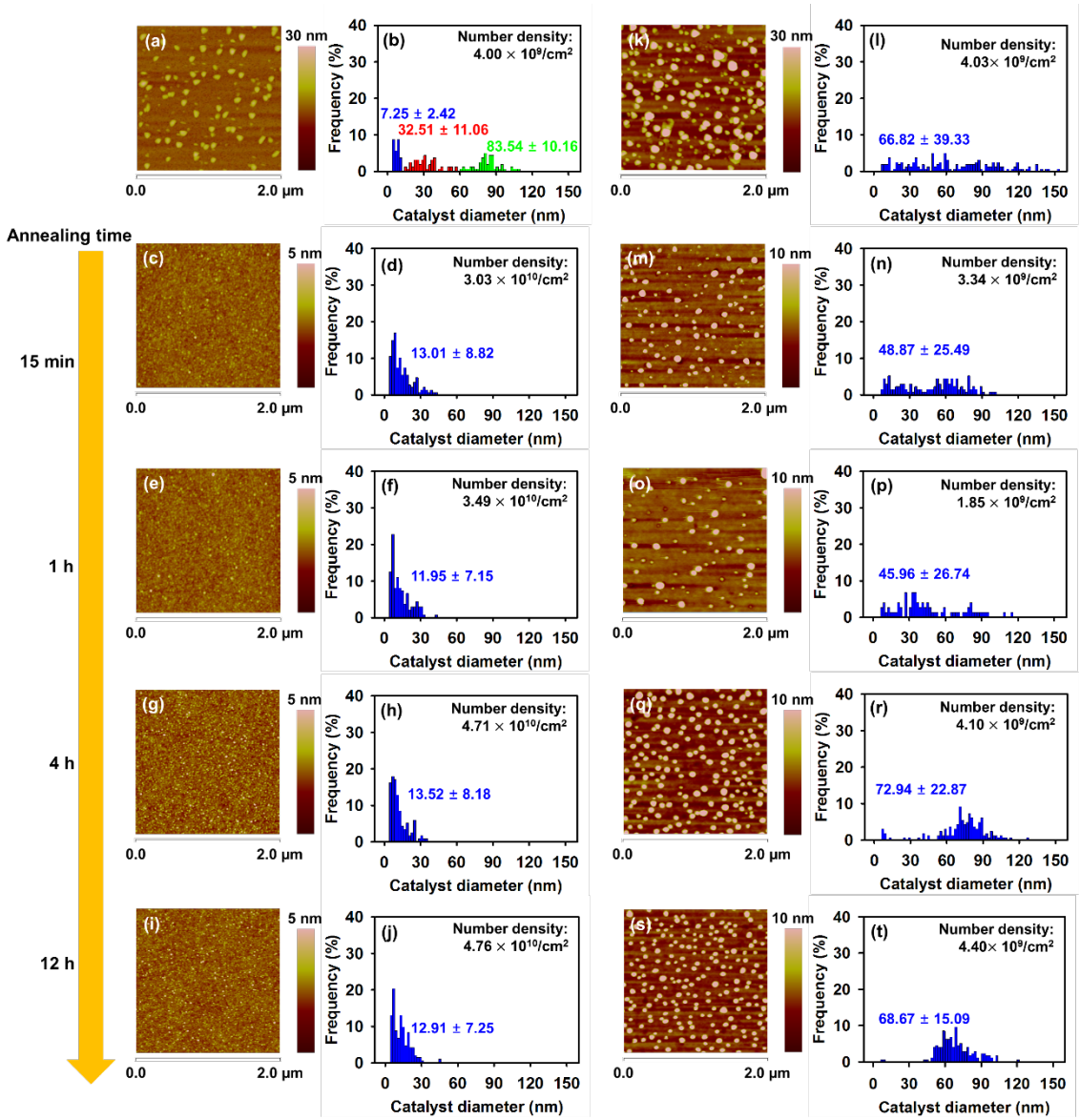

Fig. 2. Distribution of Fe catalyst particles in DWs and IWs after annealing at 800 °C. AFM images of DWs after 15 min of annealing in (a) Ar and (k) H_2; their particle size distributions ((b) and (l)). AFM images of IWs after (c) 15 min, (e) 1 h, (g) 4 h, and (i) 12 h of annealing in Ar; their corresponding particle size distributions ((d), (f), (h), and (j)). AFM images of IWs after (m) 15 min, (o) 1 h, (q) 4 h, and (s) 12 h of annealing in H_2; their corresponding particle size distributions ((n), (p), (r), and (t)).

In order to investigate the effect of ambient gas on the size distribution of Fe catalyst particles in the IWs, the annealing experiment was performed under the same conditions, except H_2 was used instead of Ar as the ambient gas. After 15 min of annealing in the H_2 atmosphere, the size

distribution of Fe catalyst particles in the DW (several nanometers to 150 nm) is even wider than that in the DW that was annealed in Ar. This is due to the high mobility of metallic particles in the H_2 atmosphere [18, 19]. For the IW samples that were annealed in H_2 for 15 min to 12 h, the number density of catalyst particles increases as the annealing time is increased from 1 h to 4 h, even though the sizes of the largest particles are very similar. However, the particle size distributions in the samples that were annealed for 4–12 h are almost the same. Moreover, the size distribution of Fe catalyst particles in the IW sample that was annealed for 12 h (Fig. 2(s) and (t)) is much narrower than that in the DW that was annealed for 15 min (Fig. 2(k) and (l)). Therefore, these annealing experiments in both Ar and H_2 ambients confirm that even after prolonged annealing for 12 h, the particle distribution in the IWs is much better maintained than that in the DW.

Since the average size, number density, and size distribution of the catalyst particles are better maintained in the IW samples that were annealed in Ar, even though the IW samples that were annealed in H_2 also show relatively narrow size distributions, the experiments presented hereafter focus on the IW samples whose annealing took place in Ar atmosphere. In order to analyze in detail the movement of Fe atoms in the IWs upon annealing in Ar, the change in the profiles of Fe atom concentration along the depth of the SiO_2 layer with increasing annealing duration was investigated by SIMS analysis; the results are shown in Fig. 3. The dose of implanted Fe^+ ions in the SiO_2 layer was $10^{16}/cm^2$. The depth profile of Fe concentration in the as-implanted sample (black squares) appears to follow a Gaussian distribution, with the maximum concentration of 1.71 $\times$ 10^{20} cm^3 at a depth of 42 nm. The concentration curve is thus fitted to a Gaussian distribution [20]. When a concentration curve follows a Gaussian lineshape, the average depth of the ions, called projected range (R_p), is given by

$$R_p = \frac{\int_{-\infty}^{\infty} xN(x)dx}{\int_{-\infty}^{\infty} N(x)dx} \ , \qquad (1)$$

where x is the depth below the surface and $N(x)$ is the Fe concentration at depth x. The variance of ion concentration is given by

$$\Delta R_p^2 = \frac{\int_{-\infty}^{\infty} (x-R_p)^2 N(x)dx}{\int_{-\infty}^{\infty} N(x)dx} \ . \quad (2)$$

The values of R_p and ΔR_p are calculated to be 54.31 and 25.38 nm, respectively. The Gaussian profile (black solid line) is obtained by substituting these values into the following equation.

$$N(x) = N_{max} \exp\left[-\frac{(x-R_p)^2}{2\Delta R_p^2}\right] \ , \qquad (3)$$

where N_{max} is the $N(x)$ at $x = R_p$ and the value is $1.56 \times 10^{20}/cm^3$. The curve fitted by a Gaussian distribution function is compared with the Fe concentration profile of the as-implanted sample in Fig. 3, and they are found to be suitable fits.

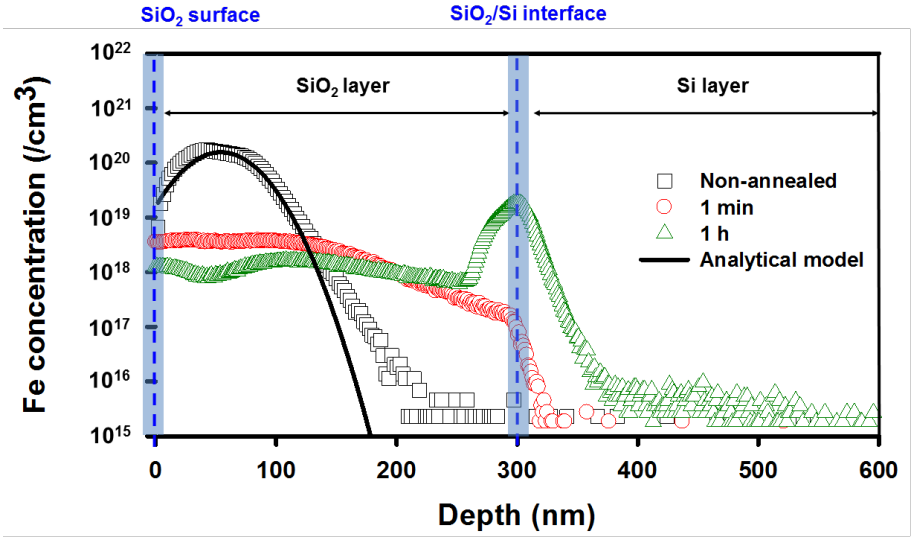

Fig. 3. Depth profile of Fe concentration in the IWs that were annealed in Ar at 800 °C; the IWs had an Fe ion dose of $10^{16}/cm^2$. Black solid line: analytical model for the as-implanted Fe ions; black squares: as-implanted Fe ions; red circles: Fe ions subjected to 1 min of annealing; green triangles: Fe ions subjected to 1 h of annealing.

When the IW samples are annealed in Ar, the depth profile of Fe concentration changes rapidly (Fig. 3). After 1 min of annealing, the concentration profile as a function of depth (red circles) becomes flat as a result of Fe diffusion in the SiO_2 layer. The area under the Fe concentration curve decreases from $1.14 \times 10^{15}/cm^2$ (as-implanted) to $6.84 \times 10^{13}/cm^2$ (after 1 min of annealing), indicating that a considerable amount of iron, which is highly strained in the SiO_2 layer [21], diffuses toward the layer's surface. After 1 h of annealing (green triangles), the Fe atoms continue to diffuse out of the SiO_2 layer and accumulate at the interface between the SiO_2 layer and Si [22, 23], while the concentration remains nearly constant in the region at a depth of 40–260 nm. The pileup of Fe at the interface is attributed to energetic preference of forming Fe clusters at the SiO_2/Si interface [24, 25].

In order to further investigate how the Fe atoms are distributed and how they diffuse through the SiO_2 layer upon heating in Ar, the cross sections of an as-implanted IW sample and an IW sample that was annealed for 12 h were analyzed by TEM (Fig. 4). Fig. 4(a)–(d) display cross-

sectional TEM images of the as-implanted sample with an Fe ion dose of $10^{16}/cm^2$. When the Fe ions are implanted, Fe atoms coalesce into small Fe particles that are then distributed in colloidal form throughout the SiO_2 layer. Since the standard free energy of formation of SiO_2 is lower than that of iron oxides such as Fe_2O_3 and Fe_3O_4 [26], the stronger bonds between Si and O prevent the Fe atoms from forming iron oxides. Thus, it is energetically favorable for the Fe atoms to form Fe colloidal particles rather than to replace Si in SiO_2 and break the bond between Si and O [26]. Fig. 4(e)–(h) show cross-sectional TEM images of the IW sample after 12 h of annealing in Ar at 800 °C. According to the SIMS analysis (Fig. 3), when the IW sample is heated in Ar, the Fe particles diffuse in two directions: toward the surface of the SiO_2 layer and the SiO_2/Si interface. This finding is confirmed by the cross-sectional TEM images. The number density of Fe particles in the middle of the SiO_2 layer decreases (Fig. 4(c) and (g)), and the Fe particles migrate to the surface of the SiO_2 layer and the SiO_2/Si interface (Fig. 4(f) and (h)), where they agglomerate to form larger particles (Fig. 4(f) and (h)). The larger particles at the surface of the SiO_2 layer do not seem to entirely escape to the surface, but they remain anchored in the SiO_2 layer and are slightly exposed to the exterior like floating icebergs. Therefore, they are expected to have lower mobility, which explains the near invariance of the particle size distributions in the IW samples after thermal annealing.

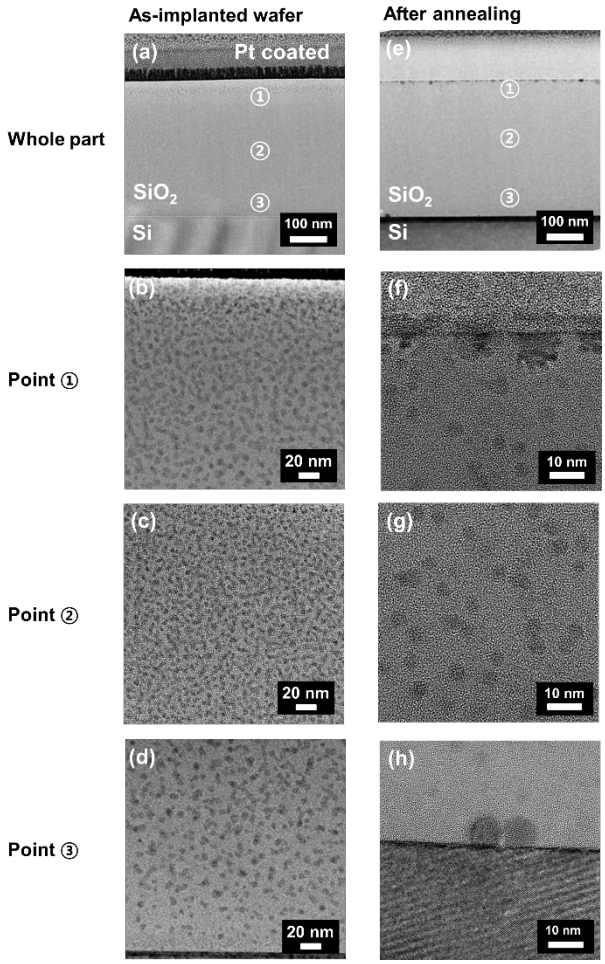

Fig. 4. (a) Cross-sectional TEM image of the as-implanted sample with an Fe ion dose of 10^{16}/cm^2; higher-magnification images at the (b) upper, (c) middle, and (d) lower sections marked as 1, 2, and 3, respectively, in (a). (e) Cross-sectional TEM image of the IW sample with an Fe ion dose of 10^{16}/cm^2 after 12 h of annealing in Ar at 800 °C; higher-magnification images at the (f) upper, (g) middle, and (h) lower sections marked as 1, 2, and 3, respectively, in (e).

The overall picture of the behavior of implanted Fe ions in the SiO_2 layer upon annealing is schematically represented in Fig. 5. When Fe ions are implanted into the SiO_2 layer on Si, the Fe ions tend to aggregate with each other rather than atomically disperse in the SiO_2 layer. Therefore, Fe particles or clusters are distributed in colloidal form in the SiO_2 layer and the depth profile of Fe concentration clearly follows a Gaussian distribution. However, as the IW samples are annealed at temperatures high enough for the Fe particles to become mobile, they move toward the surface of the SiO_2 layer and the interface between SiO_2 and Si, forming larger particles. The Fe particles near the surface are anchored and tightly bound to the SiO_2 layer, enabling the Fe particle size

distribution to be nearly uniform after prolonged annealing durations of up to 12 h.

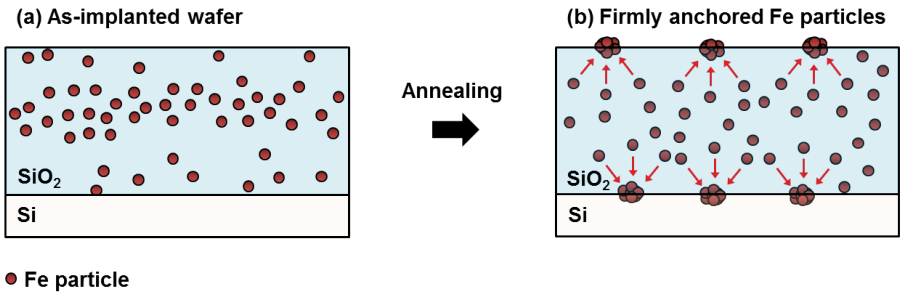

Fig. 5. Schematic representations of Fe particle distribution in the (a) as-implanted sample and (b) IW sample after annealing.

Since the diameter of the implanted Fe particles on the surface of the substrate is well maintained during thermal treatment, the CNTs grown on an IW are expected to have a more uniform diameter distribution than that of CNTs grown on a DW. The correlation between the catalyst size and CNT diameter was investigated by growing CNTs using a DW and multiple IWs. For this experiment, the DW and IWs were first annealed in Ar at 800 °C for the designated durations. The CNT forests were then grown under the same conditions on the annealed DW and IWs. For the IWs that were annealed for different durations (from 15 min to 12 h), CNT forests whose height range from 15 to 40 μm were produced after 3 min of growth at 630 °C. Representative SEM images of the CNT forests grown on the IW that was annealed for 1 h are shown in Fig. 6(a) and (b). The diameters and number of walls of the as-synthesized CNTs were analyzed by TEM, and the results are shown in Fig. 6(c) and 6(d). The diameter distributions of the as-synthesized CNTs are plotted as histograms in Fig. 6(e). It is clearly observed that even though the DW was annealed for only 15 min, the CNTs synthesized on the DW have a range of diameters. On the contrary, the CNTs synthesized on the IWs have smaller diameters with a more uniform distribution, and the diameter distributions of CNTs grown on the IWs that were annealed for 15 min, 1 h, 4 h, and 12 h are almost identical. The average diameter of CNTs synthesized on the IWs ranges from 7.40 to 8.85 nm and the standard deviation is only 1–2 nm, while that of CNTs grown on the DW is 16.65 nm with a standard deviation of 7.3 nm. These results are in good agreement with the Fe particle size distributions shown in Fig. 2 because the diameter of the CNTs is strongly correlated with the size of the catalyst particles. These results confirm that the implantation method is very useful for growing CNTs with a narrow diameter distribution when compared to the conventional PVD

method, although the alignment and the diameter distribution of CNTs from DW can be improved by using the optimized growth conditions.

The implantation method would be more beneficial than the PVD method for growing tall CNT forests over longer growth durations. Several studies have reported that the length limitation of long CNT forest growth results from catalyst depletion due to Ostwald ripening, sub-surface diffusion, and upward migration [2, 3], which eventually leads to CNT density decay and growth termination [8]. Obviously, more detailed analysis in Fe catalyst morphology and the optimization of CNT forest growth are necessary, but we believe that the implantation method would help to maintain the number density of catalyst particles and extend the growth period during the cultivation of tall CNT forests. In addition, the formation of small and uniformly sized catalyst particles by ion implantation method would be beneficial for the growth of horizontally aligned single-walled CNTs on a quartz substrate with narrow diameter distribution, if the amount of Fe ion dose and the catalyst forming step as well as CNT growth conditions can be optimized.

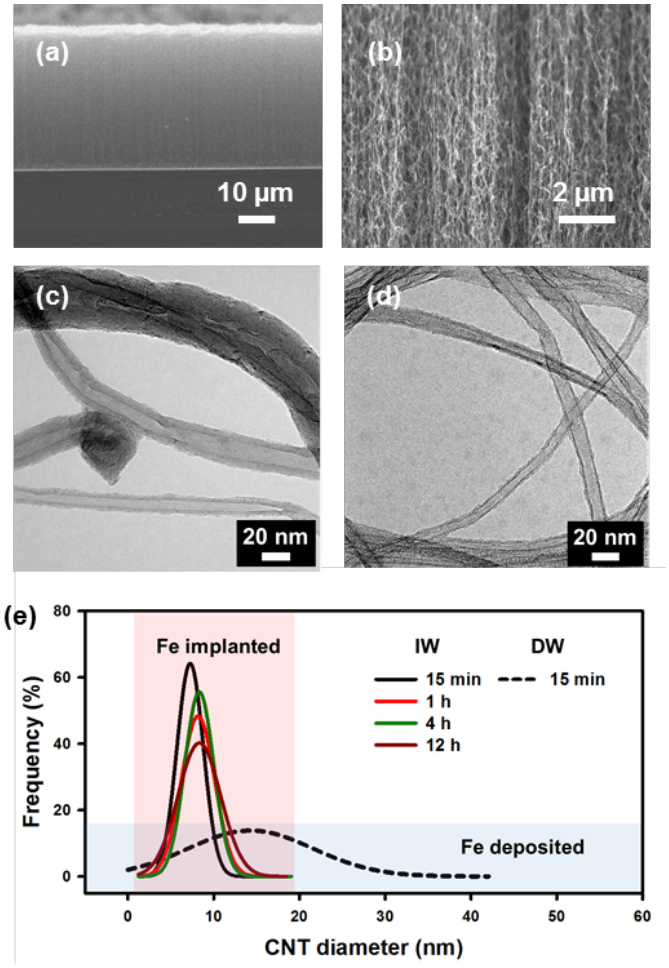

Fig. 6. (a) Representative SEM image of a CNT forest obtained on an IW after it was annealed for 1 h in Ar; (b) magnified SEM image of the CNT forest in (a). TEM images of CNTs obtained on (c) a DW and (d) an IW after they were annealed for 15 min. (e) Diameter distribution curves of CNTs synthesized on the DW (a dashed line) and the IWs (solid lines) that were annealed for various durations.

- Towards immortal catalysts: growth of centimeter-tall CNT forests using Fe-implanted substrates

It is known that a significant amount of catalysts are lost by sub-surface diffusion during the growth of a CNT forest, and this causes growth termination of a CNT forest. To overcome this problem, a new catalyst design is proposed. We first implanted Fe ions into Al_2O_3 (10 nm, deposited by atomic layer deposition) / SiO_2 (300 nm) /Si wafer at a dose of $10^{16}/cm^2$. Then, we deposited thin Fe film on the Fe-implanted wafer. We hypothesized that the Fe particles in the Al_2O_3 layer suppress the sub-surface diffusion by reducing the Fe concentration gradient in the vertical direction. This idea is schematically presented in Fig. 7, where Fe particle distributions during CNT forest growth in the DW and Fe-implanted-and-deposited wafer (hereafter referred to as IDW) are described.

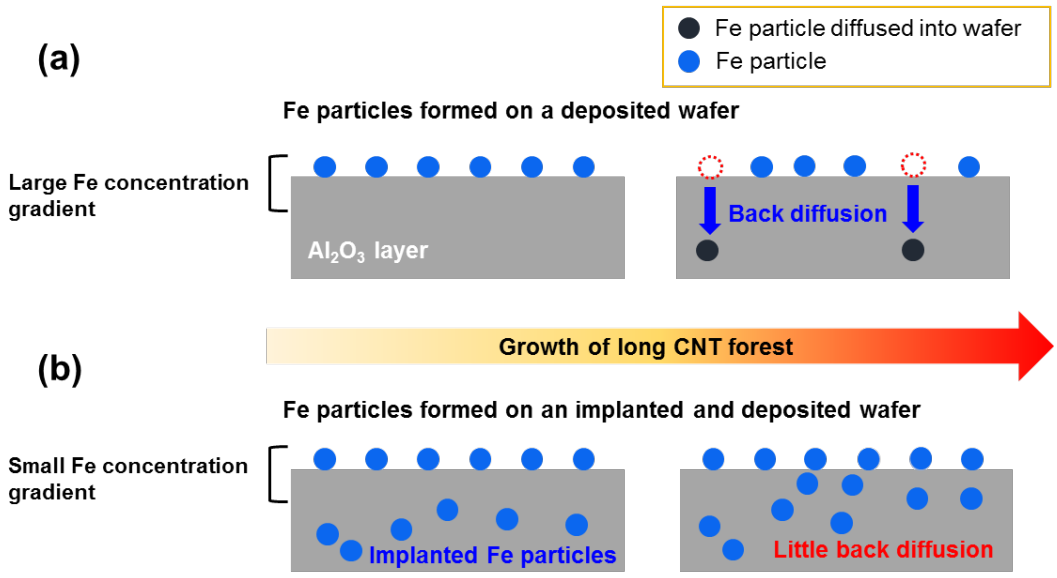

Fig. 7. Schematic representations of Fe particle distribution during CNT forest growth in the (a) DW and (b) IDW.

The location of Fe particles after the growth of CNT forests was observed by TEM. Fig. 8(a) and (b) are cross-sectional TEM images of DW and IDW after 11 h of CNT forest growth. For a clear observation of substrate, CNTs were removed prior to sampling. In DW, some Fe particles are located underneath Al_2O_3 layer as a result of sub-surface diffusion (Fig. 8(a)). On the contrary, in IDW, no Fe particle was observed underneath Al_2O_3 layer (Fig. 8(b)). Fig. 8(c) shows growth curves of CNT forests from DW and IDW. In the case of DW, the growth was decelerated after 300 min of growth, but in the case of IDW, the growth rate was relatively well maintained until the growth was terminated by the limited space in the quartz tube whose inner diameter was 1 inch. Thus, the implanted Fe particles in the Al_2O_3 layer suppressed the sub-surface migration of Fe particles on the surface and contributed to the enhanced catalytic activity for such a long growth duration.

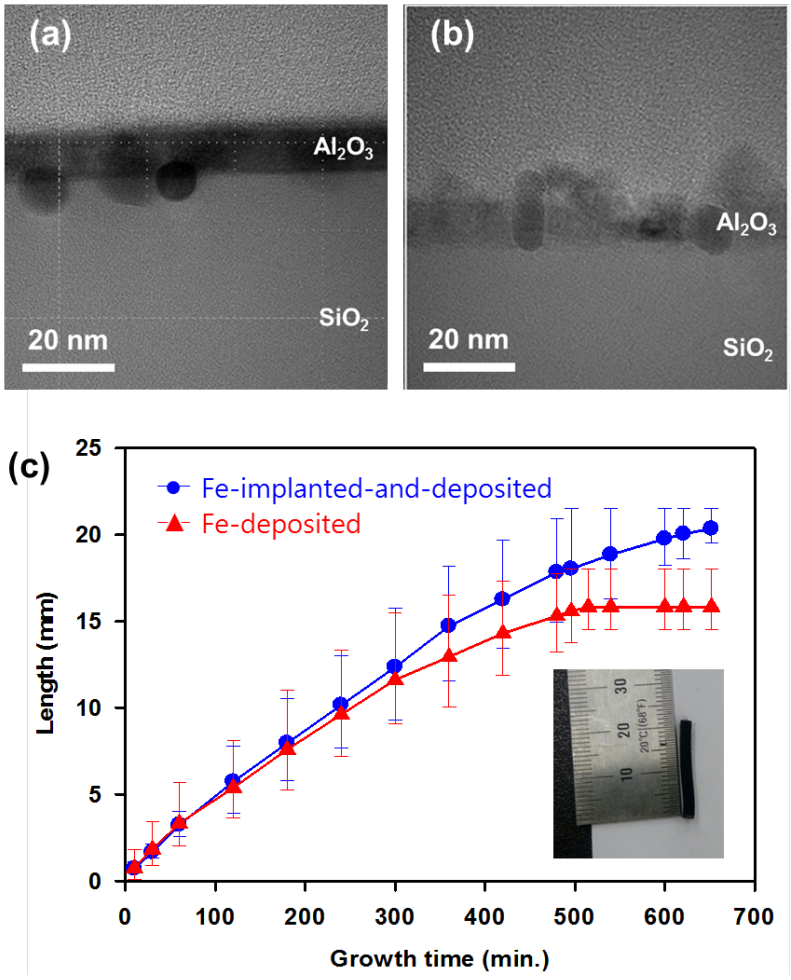

Fig. 8. Cross-sectional TEM images of (a) DW and (b) IDW after CNT growth. (c) Growth curves of CNT forests on a DW and an IDW. The inset in (c) is an image of a 21-mm-tall CNT forest.

References

[1] Amama PB, Pint CL, McJilton L, Kim SM, Stach EA, Murray PT, et al. Role of Water in Super Growth of Single-Walled Carbon Nanotube Carpets. Nano Lett. 2009;9(1):44-9.
[2] Kim SM, Pint CL, Amama PB, Zakharov DN, Hauge RH, Maruyama B, et al. Evolution in Catalyst Morphology Leads to Carbon Nanotube Growth Termination. The Journal of Physical Chemistry Letters. 2010;1(6):918-22.
[3] Jeong S, Lee J, Kim H-C, Hwang JY, Ku B-C, Zakharov DN, et al. Direct observation of morphological evolution of a catalyst during carbon nanotube forest growth: new insights into growth and growth termination. Nanoscale. 2016;8(4):2055-62.
[4] Polsen ES, Bedewy M, Hart AJ. Decoupled control of carbon nanotube forest density and diameter by continuous-feed convective assembly of catalyst particles. Small. 2013;9(15):2564-75.
[5] Lee CJ, Lyu SC, Cho YR, Lee JH, Cho KI. Diameter-controlled growth of carbon nanotubes using thermal chemical vapor deposition. Chemical physics letters. 2001;341(3):245-9.
[6] Jung D, Kim J-h, Lee KH, Overzet LJ, Lee GS. Effects of pre-annealing of Fe catalysts on growth of spin-capable carbon nanotubes. Diamond and Related Materials. 2013;38:87-92.
[7] Flynn PC, Wanke SE. A model of supported metal catalyst sintering: I. Development of model. Journal of Catalysis. 1974;34(3):390-9.
[8] Bedewy M, Meshot ER, Guo H, Verploegen EA, Lu W, Hart AJ. Collective Mechanism for the Evolution and Self-Termination of Vertically Aligned Carbon Nanotube Growth. The Journal of Physical Chemistry C. 2009;113(48):20576–82.
[9] Zhang Y, Gregoire JM, Dover RBv, Hart AJ. Ethanol-Promoted High-Yield Growth of Few-Walled Carbon Nanotubes. J Phys Chem C. 2010;114:6389-95.
[10] Arai M, Ishikawa T, Nishiyama Y. Surface migration of nickel on carbon, silicon dioxide, and aluminum oxide. The Journal of Physical Chemistry. 1982;86(4):577-81.
[11] Flynn PC, Wanke SE. A model of supported metal catalyst sintering: II. Application of model. J Catal. 1974;34(3):400-10.
[12] Granqvist C, Buhrman R. Size distributions for supported metal catalysts: Coalescence growth versus ostwald ripening. Journal of Catalysis. 1976;42(3):477-9.
[13] Granqvist C, Buhrman R. Log-normal size distributions of ultrafine metal particles. Solid State Communications. 1976;18(1):123-6.
[14] Wynblatt P, Gjostein N. Supported metal crystallites. Progress in solid state chemistry. 1975;9:21-58.
[15] Leveneur J, Waterhouse GI, Kennedy J, Metson JB, Mitchell DR. Nucleation and growth of Fe nanoparticles in SiO2: a TEM, XPS, and Fe L-edge XANES investigation. The Journal of Physical Chemistry C. 2011;115(43):20978-85.
[16] Strobel M, Heinig K-H, Möller W, Meldrum A, Zhou D, White C, et al. Ion beam synthesis of gold nanoclusters in SiO 2: computer simulations versus

experiments. Nuclear Instruments and Methods in Physics Research Section B: Beam Interactions with Materials and Atoms. 1999;147(1):343-9.
[17] Oyoshi K. Migration of ion-implanted Fe in silica glass during thermal treatment. Japanese journal of applied physics. 2002;41(10R):6145.
[18] Lee IH, Han GH, Chae SJ, Bae JJ, Kim ES, Kim SM, et al. Criteria for Producing Yarns from Vertically Aligned Carbon Nanotubes. Nano. 2010;5(1):31-8.
[19] Zhang Y, Zou G, Doorn SK, Htoon H, Stan L, Hawley ME, et al. Tailoring the Morphology of Carbon Nanotube Arrays: From Spinnable Forests to Undulating Foams. Acs Nano. 2009;3(8):2157-62.
[20] Suzuki K. Ion Implantation and Activation. first ed. U.A.E., Sharjah: Bentham Science Publisheres Ltd; 2013.
[21] Kononchuk O, Korablev K, Yarykin N, Rozgonyi G. Diffusion of iron in the silicon dioxide layer of silicon-on-insulator structures. Applied physics letters. 1998;73(9):1206-8.
[22] Hoshino Y, Yokoyama A, Yachida G, Nakata J. Analysis of depth redistribution of implanted Fe near SiO 2/Si interface. Nuclear Instruments and Methods in Physics Research Section B: Beam Interactions with Materials and Atoms. 2013;314:140-3.
[23] Ohsawa A, Honda K, Toyokura N. Metal Impurities near the SiO2-Si Interface. Journal of the Electrochemical Society. 1984;131(12):2964-9.
[24] Ramappa DA, Henley WB. Diffusion of iron in silicon dioxide. Journal of the Electrochemical Society. 1999;146(10):3773-7.
[25] Kamiura Y, Hashimoto F, Iwami M. Observation of iron pileup and reduction of SiO2 at the Si-SiO2 interface. Applied physics letters. 1988;53(18):1711-3.
[26] Hosono H. Simple criterion on colloid formation in SiO2 glasses by ion implantation. Japanese journal of applied physics. 1993;32(9R):3892.

List of Publications and Significant Collaborations that resulted from your AOARD supported project:

- Cheol-Hun Lee,† Jaegeun Lee,† Sunmog Yeo, Sung-Hyun Lee, Teawon Kim, Hyeon-Gu Cha, Youngmoo Eun, Hyun Jin Park, Seung Min Kim*, and Kun-Hong Lee*, “Synthesis of CNT forest with narrow diameter distribution from the Fe ion implanted wafer”, ***Carbon***, vol. 123, pp. 122-128 (2017) (†equal contributor)